Stem Cell Research & Therapy

RESEARCH

Open Access

# Synergistic promotion of bone regeneration through co-culture of endothelial cells with mesenchymal stem cells in endochondral ossification organoids

Yiqi Su[1,2†], Zihao He[1,2†], Jiaojiao Li[3], Qianqian Chen[4], Du Wang[1,2], Zhen Yang[1,2], Ye Yuan[1,2], Long Chen[1,2], Fanhao Ye[1,2], Dan Xing[1,2*], Hui Li[1,2*] and Jianhao Lin[1,2*]

## Abstract

**Background** Endochondral ossification (ECO) is essential for bone regeneration, involving cartilage formation, hypertrophy, angiogenesis, and ossification. Co-culturing mesenchymal stem cells (MSCs) with endothelial cells (ECs) shows potential to enhance bone regeneration but has not been effectively applied to ECO strategy.

**Methods** We examined the synergistic effects of MSCs and ECs on chondrogenesis, osteogenesis, and angiogenesis, followed by transcriptomic analysis. ECO organoids were formed in the scaffolds, and a critical-sized calvarial bone defect model was used for in vivo evaluation.

**Results** Co-culture of ECs and MSCs promoted osteogenic differentiation and hypertrophic chondrogenic differentiation of MSCs. The ECO organoids exhibited enhanced vascularization and improved mineralization. In vivo, the co-culture group showed superior vascularization and bone repair compared to the MSCs-only group.

**Conclusions** Co-culturing ECs with MSCs in ECO organoids enhances bone regeneration, offering a promising alternative to traditional tissue engineering strategies. This approach may improve therapeutic outcomes by promoting endochondral bone formation.

**Keywords** Bone repair, Endochondral ossification, Mesenchymal stem cells, Endothelial cells, Organoid

†Yiqi Su and Zihao He contributed equally to this work.

*Correspondence:
Dan Xing
xingdan@bjmu.edu.cn
Hui Li
doctor_li@bjmu.edu.cn
Jianhao Lin
linjianhao@pkuph.edu.cn

[1]Arthritis Clinic & Research Center, Peking University People's Hospital, Peking University, Beijing 100044, China
[2]Arthritis Institute, Peking University, Beijing 100044, China
[3]School of Biomedical Engineering, Faculty of Engineering and IT, University of Technology Sydney, Sydney, NSW 2007, Australia
[4]Third Clinical College, Zhejiang Chinese Medical University, Hangzhou 310053, China

## Introduction

Endochondral ossification (ECO) is the primary process responsible for bone formation during prenatal development and bone repair after injury in adults [1–3]. ECO begins with the formation of a hyaline cartilage template, which undergoes hypertrophy and calcification, followed by invasion of blood vessels and subsequent deposition of mineralized bone. In this process, vascularization plays a key role by providing the necessary oxygen and nutrients for new bone formation [4], as well as facilitating the transition from the activities of hypertrophic chondrocytes to osteoprogenitor cells and osteoclasts, which remodel the calcified cartilage into mineralized bone [5]. In addition, vascularization plays a crucial signaling role in bone repair by regulating osteocyte survival and differentiation [6]. In bone tissue engineering (BTE), insufficient vascularization or the lack of a vascularized network in organoids and scaffold constructs remain a significant barrier to successful bone repair, particularly in large defects [7]. Over the last two decades, studies have attempted to combine osteogenesis and angiogenesis to enhance the outcomes of bone regeneration [8–11]. These studies have noted a positive feedback mechanism known as angiogenic-osteogenic coupling, where angiogenesis promotes bone development while the formation of bone tissue reversely enhances angiogenesis [5]. However, the strategies employed by most studies involved various scaffold modifications, such as pore structure, addition of bioactive substances, and tailored surfaces, or the direct addition of angiogenic cells [12], focusing on evaluating the outcomes of bone regeneration without deep understanding of the mechanisms by which vascularization participates in bone repair. Moreover, much of the bone formation resulting from these strategies is direct and rapid, analogous to intramembranous ossification but not representative of the natural process of ECO, making it difficult to relate improved bone regeneration outcomes to physiologically relevant mechanistic insights.

Previous studies have demonstrated the in vitro interactions between mesenchymal stem cells (MSCs), as important progenitor cells in both chondrogenesis and osteogenesis, and endothelial cells (ECs) as the key cells responsible for angiogenesis, supplementing our understanding of the ECO process. ECs have been shown to promote osteogenesis in MSCs, while MSCs have been conversely shown to maintain EC phenotype and enhance their angiogenic ability [13–18]. However, the lack of biomimetic ECO models makes it challenging to recreate in vivo conditions and hence gain appreciation of cell interactions that are representative of their native behaviour. The majority of in vitro studies on ECO have been limited to 2D culture systems, restricting the extent of physiological interactions between cell types and the ability to capture dynamic changes in cell fate during ECO. Investigating the interactions between MSCs and ECs in 3D ECO models and their impact on the progression of ossification is a key step both in deepening our mechanistic understanding of the physiological process of ECO and in improving the development of therapeutic strategies for bone repair.

Among a limited number of studies which constructed 3D ECO models and attempted the incorporation of ECs [19–22], most have introduced the ECs during the late stage of cartilage-to-bone transition, into pre-formed cartilage/bone templates rather than at the initial stage of chondrogenic differentiation. However, during natural ECO, vascular invasion closely follows the first phase of cartilage differentiation, well before the late phase of bone formation. This early vascularization is critical for the subsequent progression of ECO. In an ECO model, the early introduction of ECs may be essential for enhancing blood supply and oxygen exchange within the newly formed cartilage matrix. This optimizes the microenvironment for cartilage differentiation and provides more physiologically relevant insights into the mechanisms of early vascular-cartilage interactions. Furthermore, establishing vascular networks during the early phase of ECO may create a more favourable microenvironment for subsequent ossification, facilitating accelerated mineralization and improved integration with the host vasculature. In this study, we established a 3D MSC-EC co-culture system that introduced ECs during the early chondrogenic stage, aiming to recreate a process more closely resembling natural ECO. This strategy seeks to address the limitations of existing research and may pose a solution to the common issue of "delayed vascular invasion" for implanted bone constructs [23, 24], with the potential to significantly shorten the repair timeline.

In our previous work, we established an innovative in vitro ECO organoid model using engineered MSCs and microspheres [25], which effectively simulated the in vivo process of ECO. In this study, we created a new co-culture system of MSCs and ECs based on ECO organoids, where ECs were introduced during the initial stage of chondrogenic differentiation. This integration not only enhanced cell-cell interactions but also optimized the local microenvironment, which was crucial for organoid development and function. Comprehensive evaluations of cell interactions, in vitro ECO organoid performance, and in vivo bone repair outcomes demonstrated significantly improved osteogenesis through the co-cultivation of ECs with MSCs in the ECO organoids. The findings of this study provide a realistic and comprehensive understanding of bone formation mechanisms in ECO, as well as introduce new directions for enhancing the repair outcomes of large bone injuries.

## Materials and methods

### Cell culture and identification

Human umbilical cord MSCs (UCMSCs, hereafter referred to as MSCs) were purchased from EUBIO Technologies. Human umbilical vein endothelial cells (HUVECs, hereafter referred to as ECs) and ATDC5 cells were kindly donated by the Orthopaedic Laboratory of the Ninth People's Hospital, Shanghai Jiao Tong University School of Medicine. MSCs, ECs and ATDC5 cells were grown in α-MEM medium (Gibco) containing 10% fetal bovine serum (FBS; Gibco) and 1% penicillin-streptomycin (P-S, Hyclone). When the cells were grown to 80% confluent, conditioned medium (CM) was obtained by washing the cells in phosphate buffered saline (PBS) and culturing for 48 h in fresh medium.

To identify MSC-related surface markers (Figure S1), MSCs ($1 \times 10^6$ cells) were incubated with the following monoclonal antibodies: FITC-CD45 (Biolegend), FITC-CD73 (Biolegend), APC-CD90 (Biolegend), PE-CD105 (Biolegend). Unstained cells were used as negative controls. MSCs were incubated with antibodies at room temperature for 30 min and then detected by flow cytometry (BD Biosciences).

### Cell viability and migration assay

Cell viability was measured by CCK-8 kit (Dojindo) and live/dead staining kit (Beyotime). Transwell migration was used to evaluate the effect of MSC-CM on the migration ability of ECs. ECs ($1 \times 10^4$ cells) were seeded into Transwell inserts (Corning) containing 8 μm pore membrane. In the lower culture chamber, growth medium or MSC-CM was added. After incubation for 12 h, the cells were fixed with 4% paraformaldehyde and stained with crystal violet for 5 min. The cells which have migrated to the underside of the Transwell membrane were then observed by microscopy. For the scratch healing experiment, ECs ($2 \times 10^5$) were seeded in a 6-well plate. Once the cells reached confluence, a sterile pipette tip was used for the scratch, followed by culturing the cells in growth medium or MSC-CM until the scratch was fully healed. The scratch was imaged at 0 and 24 h, and the healing area was calculated using ImageJ software.

### Tube formation assay of ECs

Matrigel (Corning) was evenly spread on 96-well plates and incubated at 37 ℃ for 30 min. An EC suspension was prepared, and the 96-well plates were inoculated with 100 μL cell suspension ($1 \times 10^4$ cells) per well. Calcein-AM staining was performed after 4 to 6 h, and microscopy images were taken. Quantitative results were calculated using the ImageJ software.

### MSC differentiation and ECO model

For osteogenic induction, osteogenic medium was α-MEM containing 10% FBS, 1% P-S, 500 μM ascorbic acid, 10 mM β-glycerophosphate, and 100 nM dexamethasone. ALP activity was evaluated on day 7, where BCIP/NBT kit (Beyotime) was used to determine A405, and BCA Protein Assay Kit (Beyotime) was used to determine A560. ALP activity was measured as A405/A560 [26]. Calcium deposition was evaluated on day 21, where 1% Alizarin Red S (ARS, Sigma-Aldrich) solution was used for staining, followed by washing with PBS until the eluent was colorless. Then, 10% CPC was added and the plate was shaken in a shaker for 30 min, before measuring A570 to quantify the amount of calcium nodules.

For chondrogenic induction, chondrogenic medium was α-MEM containing 10% FBS, 1% P-S, 10 ng/mL TGF-β3, 100nM dexamethasone, and 10μM ascorbic acid. On day 21, the cartilage pellet was fixed with 4% paraformaldehyde, followed by paraffin embedding and sectioning, and histological and immunohistochemical staining to evaluate chondrogenesis.

For the ECO model, cells were encapsulated in Col-I sponges (purchased from Wuxi BIOT Biology Technology Co., Ltd.) with dimensions of 3 mm diameter and 2 mm height. MSCs and ECs were resuspended and seeded into the scaffolds at a ratio of 9:1 within an 8 μL volume of $1 \times 10^5$ cells/μL. This induction involved two phases: chondrogenesis followed by hypertrophy. Chondrogenic medium composition was described above. Hypertrophic induction medium was α-MEM containing 50 μM L-thyroxin, 100 nM dexamethasone, 50 pg/mL IL-1β, and 0.01 M β-glycerophosphate [25]. The cell ratio was determined based on preliminary experiments (Figure S2). Specifically, we initially tested cell ratios of 1:0, 1:1, 3:1, and 9:1 (MSC: EC). After seeding the mixed cells into type I collagen scaffolds and conducting chondrogenic induction, we observed on day 3 that the 9:1 group was able to form a relatively compact spheroid, similar to the result observed in the pure MSC group. Therefore, we chose the 9:1 ratio for co-culture.

To detect the in vitro VEGFA secretion ability of ECO organoids, 15 ECO organoids (cultured for 6 weeks) were placed into Transwell inserts containing 0.4 μm pore membrane (Corning), and the bottom of the lower chamber was coated with Matrigel and seeded with ECs. After 6 h, the lower chamber was stained with Calcein-AM and microscopy images were taken. Quantitative analysis was performed using ImageJ software.

Histology, immunohistochemistry, and μ-CT scanning of ECO organoids were performed after 6 weeks of in vitro culture, using the same procedures as described later for the animal experiments.

### RT-qPCR and bulk RNA-Seq

Total RNA was extracted using TRIzol reagent (Invitrogen). The RNA was reverse transcribed into cDNA with a Prime Script RT reagent kit (Takara). Primers were synthesized by Sangon Biotech (Table S1) and GAPDH was used as an endogenous control. SYBR Green (Takara) was used to measure gene expression by RT-qPCR. Relative mRNA expression was calculated using the $2^{-\Delta\Delta Ct}$ method.

For bulk RNA-seq, the control group comprised MSCs while the experimental group comprised MSCs treated with EC-CM, with each group containing three independent replicates. RNA was first extracted using TRIzol reagent (Invitrogen), followed by the construction of a cDNA library and high-throughput sequencing. The sequencing data were then subjected to quality control and alignment, and DESeq2 was used to identify differentially expressed genes (DEGs). Subsequently, GO and KEGG enrichment analyses were performed, and gene set enrichment analysis (GSEA) was conducted to assess the enrichment of gene sets.

### Western blot

Cells were homogenized in radio immunoprecipitation assay (RIPA, Leagene). Protein concentrations were determined using the BCA Protein Assay Kit (Beyotime). Samples were loaded on 10% SDS–polyacrylamide gel electrophoresis gels and then transferred to nitrocellulose membranes. Immunoblotting was done in primary antibody dilution buffer (A1810, Solarbio) with the corresponding antibodies. The antibodies used were: VEGFA (Proteintech), CD31 (Bioss), and GAPDH (YEASON). Full-length blots are presented in Supplementary Material 2.

### Scanning electron microscopy (SEM)

The microstructural properties of microspheres were characterized by SEM (FEI Quanta 200). The microspheres were fixed with 2.5% glutaraldehyde, dehydrated and dried, and then sputter coated with gold before images were taken using SEM.

### DAPI/Phalloidine staining

The cytoskeleton of cells cultured in microspheres was analyzed by staining with Phalloidine (Beyotime) and 4′,6-diamidino-2-phenylindole (DAPI, Beyotime). The stained microspheres were observed using a TCS-SP8 STED 3X confocal microscope (Leica).

### Animal experiment

The rat calvarial defect model and associated animal experiments were conducted under the approval of the Peking University Ethics Committee (LA2019365). The work has been reported in line with the ARRIVE guidelines 2.0 (Supplementary Material 3). Sprague-Dawley (SD) rats ($n = 36$; aged 8 weeks) were randomly divided into three groups. For each animal, after full anesthesia with isoflurane, two 5 mm diameter defects were carefully created in the skull bone using a trephine bur. The dura mater was meticulously preserved to prevent hemorrhage and ensure optimal bone healing conditions. For the same group of rats, each of the three rats was randomly placed in the same cage and placed in the same location in the animal house. Post-operative care included the administration of 100 mg/kg cefazolin for two days to prevent infection. Rats were monitored daily, and all rats with infected incisions were excluded.

The three groups were: **Ctrl group** where defects were treated with empty microspheres; **MSC group** where defects were treated with microspheres loaded with $1 \times 10^6$ MSCs; and **MSC + EC group** where defects were treated with microspheres loaded with $9 \times 10^5$ MSCs and $1 \times 10^5$ ECs. Both cell-containing groups underwent 7 days of pre-culture in chondrogenic differentiation conditions before implantation. During surgery, defects were treated with the respective constructs, and the surgical site was closed with sutures.

Blinding measures were implemented at different stages of the experiment to reduce bias and enhance the reliability of the study. Group allocation was performed by YQS and ZHH using a randomization method. The experimenters responsible for outcome assessment and data analysis were blinded to the group allocation to avoid potential bias.

### Microfil perfusion and μ-CT

At 6 weeks post-surgery, half of the rats were anesthetized, and a long incision was made in the chest and abdomen to fully expose the heart and free the liver. A vascular catheter was inserted into the left ventricle, and the right auricle was broken by micro-scissors. Sequential injections of 20 mL of heparinized saline, 20 mL of 4% paraformaldehyde, and 20 mL of Microfil solution were made. Finally, the sample was left overnight at 4 °C [9, 19, 27].

At 12 weeks post-surgery, μ-CT scanning was performed after euthanizing the other half of rats with carbon dioxide ($CO_2$) gas. The excised calvarial specimens encompassing the defect area were fixed in 4% paraformaldehyde for 24 h, and subsequently assessed using μ-CT (SCANCO μCT-100, Switzerland). Parameters including bone volume/tissue volume (BV/TV), bone mineral density (BMD), and the relative bone growth surface area of the regenerated tissue were quantified using Evaluation V6.5 software (SCANCO, Switzerland).

### Histology and immunohistochemistry

The calvarial specimens were decalcified using 10% EDTA solution over a period of four weeks. Following a sequential dehydration process in graded ethanol series, the samples were embedded in paraffin and sectioned with 7 mm thickness. Staining was performed with hematoxylin and eosin (H&E), Safranin O-Fast Green, and Masson's trichrome. For immunohistochemical analysis, antibodies targeting Col-I (Novus), Col-II (Novus), Col-X (eBioscience), CD31 (Bioss), α-SMA (Proteintech), vWF (Proteintech), PD-L1 (Proteintech) and human mitochondria (Abcam) were used.

### Bone histomorphometry analysis

Bone histomorphometry was used to analyze mineralization rate. ARS (30 mg/kg) and Calcein (30 mg/kg, Sigma-Aldrich) with fluorescent labeling were injected intraperitoneally at 3 and 10 days before euthanasia, respectively. Sample collection and histological processing were performed as described above. Non-decalcified sections were observed using a fluorescence microscope (Olympus). The mineral apposition rate (MAR) was calculated as the ratio of the distance between the two fluorescent labels to the time interval between the labeling.

### Statistical analysis

All data were obtained from at least 3 independent experiments and expressed as mean ± SEM. Statistical comparisons for two groups were made using unpaired Student's t-test, while one-way ANOVA was employed for multiple group analyses, followed by post-hoc tests for detailed pairwise comparisons. These analyses were conducted using GraphPad Prism software. For ANOVA, post-hoc comparisons were performed using Tukey's multiple comparisons test to adjust for multiple comparisons. $p < 0.05$ was considered a significant difference between groups.

## Results

### Experimental design

In vitro MSC-EC interactions were primarily focused on three key biological processes: osteogenesis, chondrogenesis, and angiogenesis, which are crucial for tissue regeneration and repair. In particular, the co-culture group, where MSCs and ECs were cultured together, demonstrated significantly enhanced outcomes. These improvements were observed in both the formation of in vitro ECO organoids, which mimicked the complex structure and function of the tissue being studied, and in the in vivo repair of bone defects, where the co-culture group exhibited superior bone healing and tissue regeneration compared to other groups(Figure 1).

### MSCs promote angiogenesis of ECs

The paracrine effects of MSCs on ECs were investigated by applying the conditioned medium (CM) (Fig. 2A). MSC-CM applied to ECs promoted cell proliferation to a certain extent, as shown by CCK-8 assay and live/dead staining (Fig. 2B-C). Moreover, ECs exposed to MSC-CM displayed enhanced migration and scratch healing (Fig. 2D-E), both of which were activities associated with their angiogenic ability. Correspondingly, ECs cultured in MSC-CM showed significant upregulation of key endothelial markers (Fig. 2F-G), including VEGFA, and CD31 [28]. These findings suggest that MSCs can mutually influence ECs through paracrine signaling,

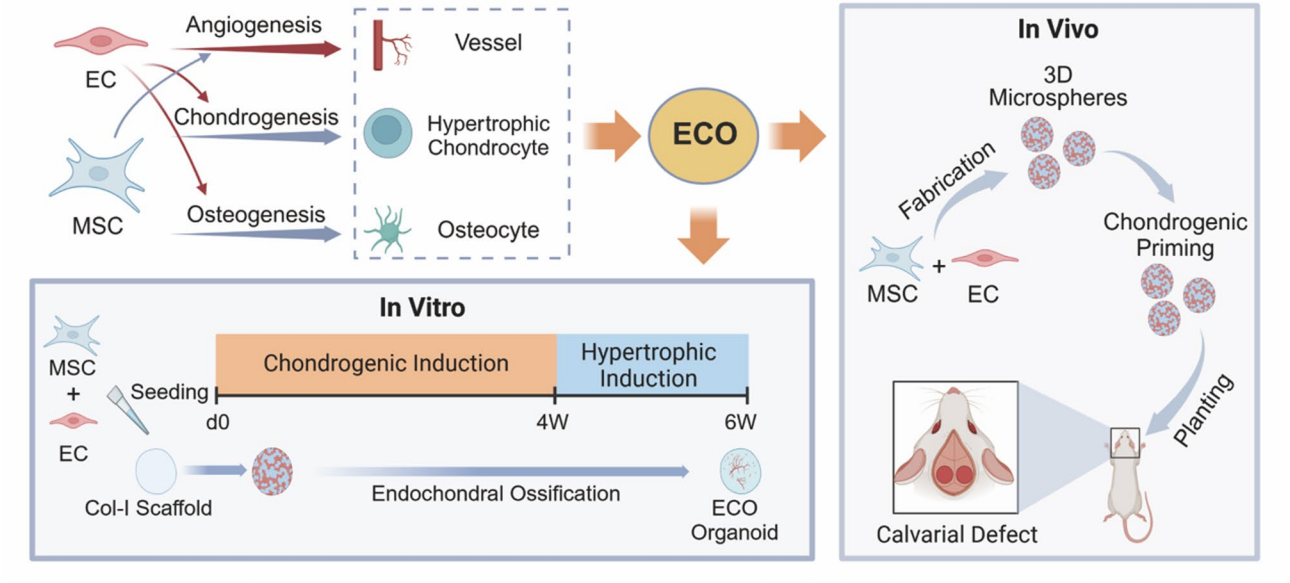


**Fig. 1** Experimental design

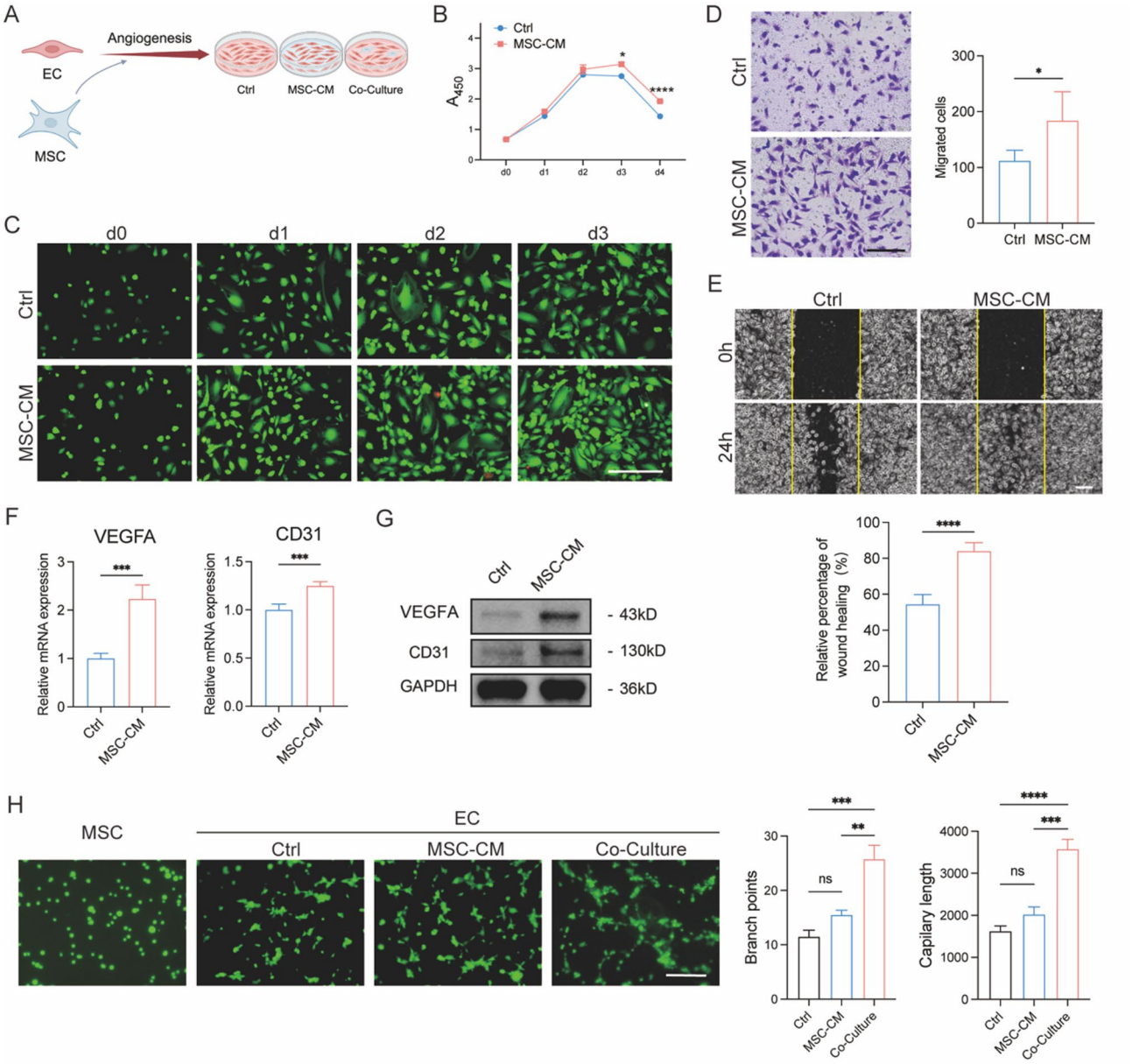


**Fig. 2** Synergistic effects of MSCs and ECs in angiogenesis. **A** Experiment set up for investigating the effect of MSCs on EC angiogenesis. **B** CCK-8 assay indicating the proliferation of ECs in response to MSC-CM. **C** Live/dead staining images of ECs after treatment with MSC-CM. **D** Transwell migration and **E** scratch healing of ECs in response to MSC-CM treatment. **F** RT-qPCR and **G** western blot analysis of endothelial marker expression in ECs after 3 days of MSC-CM stimulation. **H** Representative images and quantification of tube formation after 4 h of treatment. Scale bar = 200 μm for all microscopy images. For all charts, data are presented as mean ± SEM (standard error of the mean), * $p < 0.05$, ** $p < 0.01$, *** $p < 0.01$, **** $p < 0.0001$, ns: no significance, $n \geq 3$ per group

leading to enhanced activities related to angiogenesis. As shown in the tube formation assay of ECs, stimulation by MSC-conditioned medium (MSC-CM) slightly enhanced angiogenesis although without significant differences. In contrast, direct co-culture of ECs and MSCs at a ratio of 9:1 significantly promoted the angiogenic response (after excluding MSCs cultured alone), suggesting that a mixed culture of the two cell types may be necessary for the practical enhancement of angiogenic outcomes (Fig. 2H).

### ECs promote osteogenic differentiation of MSCs and formation of hypertrophic cartilage

The role of ECs in osteogenic differentiation of MSCs was examined by both indirect exposure through EC-CM and direct exposure through mixed co-culture at a ratio of 9:1 (Fig. 3A). Osteogenesis outcomes included ALP activity on day 7 of osteogenic induction (Fig. 3B and D) and ARS staining on day 21 (Fig. 3C and E). While exposure to EC-CM did not lead to increased ALP activity

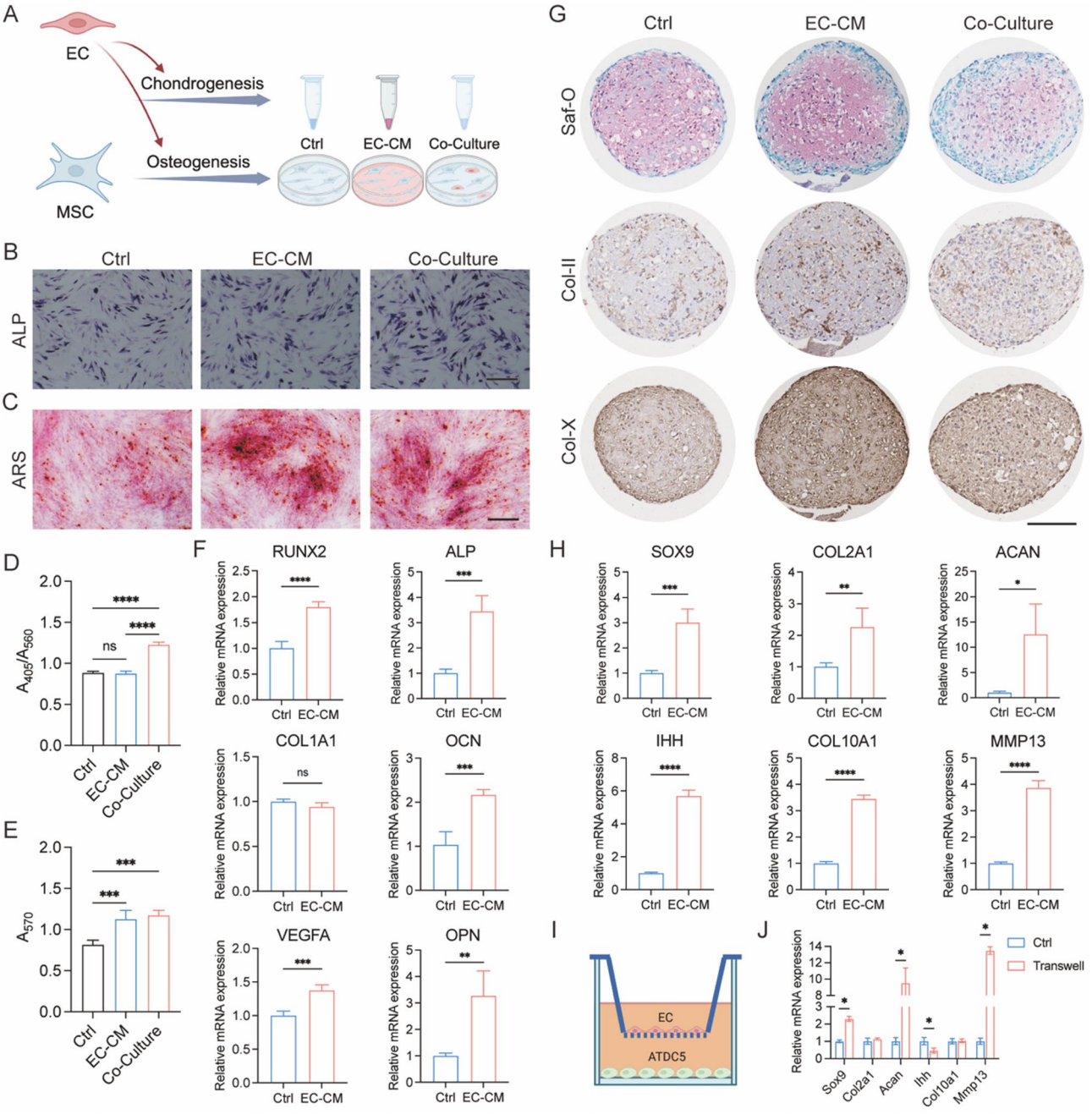


**Fig. 3** Effects of ECs on osteogenesis and chondrogenesis of MSCs. **A** Experiment set up for investigating the effects of ECs on MSC osteogenic and chondrogenic differentiation. **B** Representative images of osteogenic MSCs stained for ALP activity on day 7. **C** Representative images of osteogenic MSCs stained ARS on day 21. **D** ALP quantification on day 7 of osteogenic differentiation. **E** Calcium quantification on day 21 of osteogenic differentiation. **F** RT-qPCR results of osteogenic gene expression in MSCs on day 14 of osteogenic differentiation. **G** Representative histological (Saf-O) and immunohistochemical (Col-II, Col-X) staining of MSC chondrogenic pellets on day 21 of chondrogenic differentiation. **H** RT-qPCR results of chondrogenic gene expression in MSCs on day 14 of chondrogenic differentiation. **I** Transwell co-culture set up of ECs and ATDC5. **J** RT-qPCR results of gene expression related to cartilage metabolism in ATDC5 cells after Transwell co-culture with ECs for 3 days. Scale bar = 200 μm for all microscopy images. For all charts, data are presented as means ± SEM (standard error of the mean), * $p < 0.05$, ** $p < 0.01$, *** $p < 0.01$, **** $p < 0.0001$, ns: no significance, $n \geq 3$ per group

in MSCs, it resulted in significantly higher ARS staining indicative of a greater number of mineralized nodules. Meanwhile, MSCs directly mixed with ECs in the co-culture group showed significant elevation in both ALP activity and mineralized nodule formation. Furthermore, MSCs exposed to EC-CM were found to have greatly upregulated expression of key osteogenic genes at 14 days, including RUNX2, ALP, VEGFA, OCN, and OPN (Fig. 3F). These findings collectively suggest that ECs

have an important role in promoting the osteogenic differentiation of MSCs.

Similarly, the role of ECs in chondrogenic differentiation of MSCs was examined by indirect exposure through EC-CM and directly mixed co-culture at a ratio of 9:1. These experiment set ups were possible as our preliminary experiments confirmed that chondrogenic induction medium did not adversely affect ECs, and in fact upregulated VEGFA expression (Figure S3). The chondrogenic pellets formed by MSCs were analyzed by RT-qPCR at 14 days and histological staining at 21 days. Histological and immunohistochemical analysis revealed significantly increased expression of Col-X in both the EC-CM and direct co-culture groups compared to control pellets, with more pronounced staining observed in the EC-CM group (Fig. 3G). Interestingly, MSC pellets exposed to EC-CM showed simultaneous upregulation of both chondrogenesis-specific genes (SOX9, COL2A1, ACAN) and hypertrophic chondrocyte genes (IHH, COL10A1, MMP13) (Fig. 3H). Notably, although MMP13 is a matrix-degrading enzyme, its upregulation facilitates the remodeling of the cartilage matrix and subsequent vascular invasion, thereby creating a favorable environment for subsequent bone formation. These results suggested that ECs might help induce early chondrogenic differentiation of MSCs but eventually directs them to form hypertrophic cartilage. To verify these findings, a Transwell co-culture system was established using ECs in the top chamber and ATDC5 in the bottom chamber, both two types of cells cultured in α-MEM with 10% FBS and 1% P-S (Fig. 3I). ATDC5 is a commonly used chondrogenic cell line that has been used to model endochondral ossification and matrix mineralization [29, 30]. The early expression of genes related to cartilage metabolism in ATDC5 (Fig. 3J) corroborated with gene expression patterns in MSCs, where the co-culture group showed simultaneous upregulation of genes associated with chondrogenesis (e.g., Sox9, Acan) as well as hypertrophy and matrix degradation (e.g., Mmp13).

#### Transcriptomic analysis of MSCs exposed to EC-CM

Transcriptomic analysis was performed to compare the transcriptional profile of MSCs before and after EC-CM stimulation for 3 days. The gene expression patterns of the Ctrl and EC-CM groups were distinguished by PCA (Fig. 4A). A total of 1449 differentially expressed genes (DEGs) were detected, of which 517 were upregulated and 932 were downregulated (Fig. 4B, C). GO enrichment analysis highlighted changes in gene expression of the EC-CM group associated with osteogenesis, chondrogenesis, angiogenesis, and extracellular matrix (ECM) (Fig. 4D). Notably, KEGG enrichment analysis revealed significant differences in the expression of TGF-β and PI3K-AKT signaling pathways (Fig. 4E). Compared with the control group, the PI3K-AKT pathway related to osteogenic differentiation [31] was upregulated in the EC-CM group (Fig. 4F), while the TGF-β pathway closely related to chondrogenesis [32] as downregulated (Fig. 4G). In the early stages of chondrogenic differentiation, TGF-β signaling is not required to initiate chondrogenesis, but limits chondrogenesis for osteoblast lineage commitment. Therefore, downregulated TGF-β signaling may favor the transition from chondrocyte to osteoblast lineage [33]. These findings provide some insights into the mechanisms by which EC-CM may influence MSC differentiation and fate.

To confirm the involvement of the above identified signaling pathways, the protein expression of downstream molecules of relevant pathways was compared between the Ctrl and EC-CM groups. It was found that during osteogenic differentiation, the EC-CM group had significantly higher expression of phosphorylated AKT protein compared to the Ctrl (Fig. 4H). Since PI3K activation phosphorylates the downstream molecule AKT and causes its localization to the cell membrane, which then acts to promote bone formation [34], the elevated expression of phosphorylated AKT in the EC-CM group verifies that PI3K-AKT could be a key pathway by which ECs promote osteogenic differentiation of MSCs. Meanwhile during chondrogenic differentiation, the EC-CM group did not show enhanced phosphorylation of SMAD-2/3 as the classical downstream signal transduction molecule of TGF-β, but rather significantly increased the expression of phosphorylated SMAD-1/5/9 (Fig. 4I). This signified the activation of SMAD-1/5/9 which is reported to be associated with terminal differentiation and mineralization [35]. Combined with the results of transcriptomic analysis, these findings suggest that the EC secretome may impact MSC differentiation through different pathways, including the activation of PI3K-AKT to enhance osteogenesis, and acting through TGF-β to activate SMAD-1/5/9 signaling that promotes hypertrophy following chondrogenesis.

#### Construction of in vitro ECO organoid through extended MSC-EC co-culture in scaffolds

The above findings illustrated that ECs and MSCs influence each other through paracrine mechanisms, impacting the outcomes of MSC differentiation that allude to the process of ECO. However, short-term co-culture to a period not exceeding 3 weeks and in 2D restrict the extent of interactions between cell types as well as the ability to observe transitional and late-stage differentiation outcomes. To more faithfully mimic the physiological progression of ECO, we constructed an in vitro ECO model that uniquely involved the early introduction of ECs to MSCs, which were grown within a 3D scaffold for an extended period analogous to the time frame of

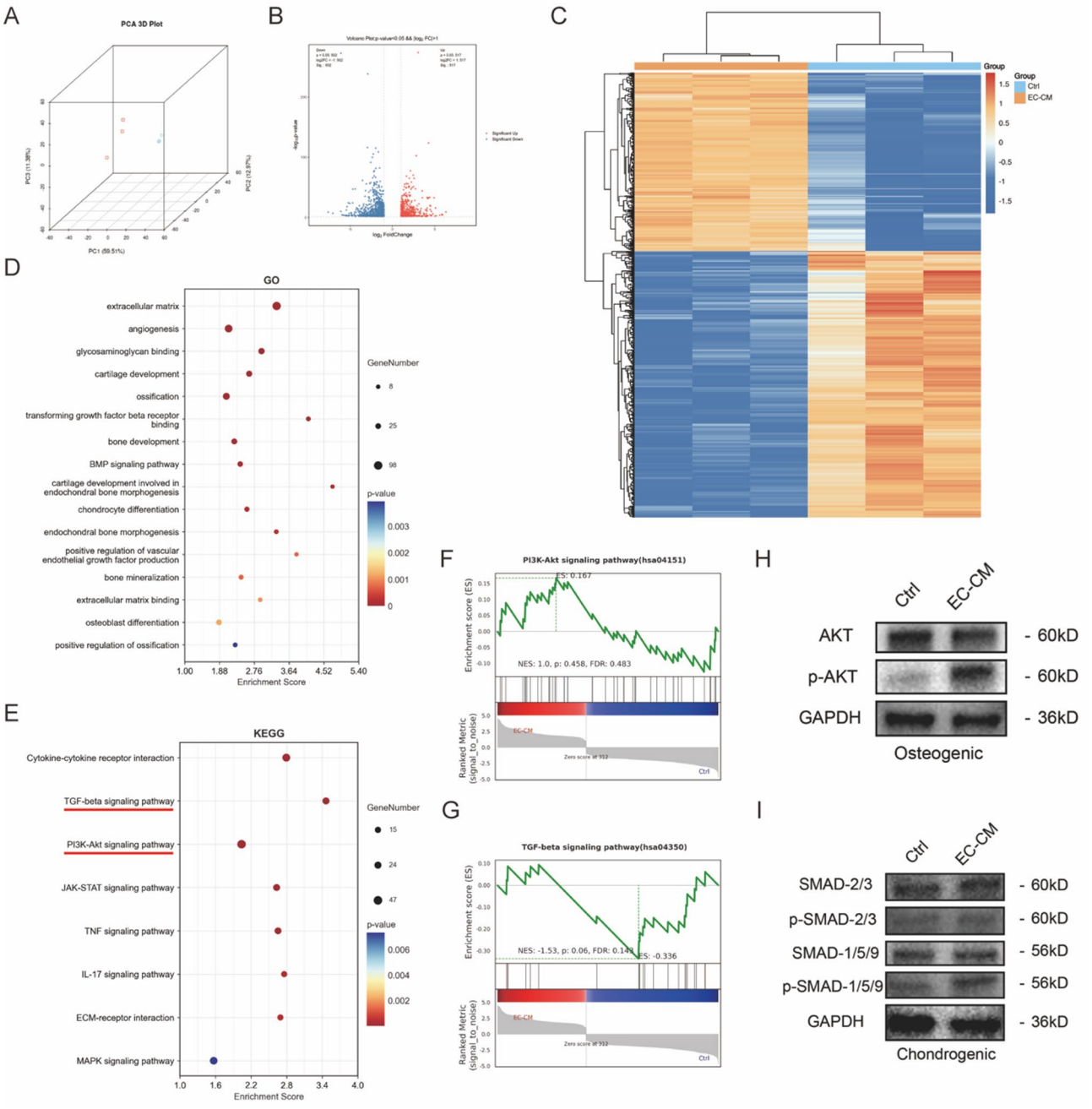


**Fig. 4** Transcriptome sequencing and signaling pathway analysis. **A** Principal Component Analysis (PCA) plot illustrating the global gene expression differences between MSCs exposed to EC-CM or not exposed (Ctrl). **B** Volcano map of differentially expressed genes (DEGs). **C** Clustering heat map of DEGs. **D** GO enrichment analysis. **E** KEGG enrichment analysis. **F** GSEA analysis of PI3K-AKT signaling pathway. **G** GSEA analysis of TGF-β signaling pathway. **H** Western blot analysis showing the protein expression of phosphorylated (p-AKT) or non-phosphorylated (AKT) downstream molecule of PI3K-AKT signaling during osteogenic differentiation of MSCs on day 3. **I** Western blot analysis showing the protein expression of phosphorylated (p-SMAD-1/5/9 and p-SMAD-2/3) or non-phosphorylated (SMAD-1/5/9 and SMAD-2/3) downstream molecule of TGF-β signaling during chondrogenic differentiation of MSCs on day 3

in vivo ECO. Specifically, MSCs and ECs at a ratio of 9:1 were seeded into type I collagen sponges, and these scaffold constructs were subjected to chondrogenic induction for 4 weeks followed by hypertrophic induction for 2 weeks, ultimately yielding in vitro ECO organoids at the end of a 6-week culture period (Fig. 5A).

After the first 4 weeks of chondrogenic differentiation, the Saf-O staining indicated that the MSC group had more hyaluronic cartilage matrix, while the MSC + EC

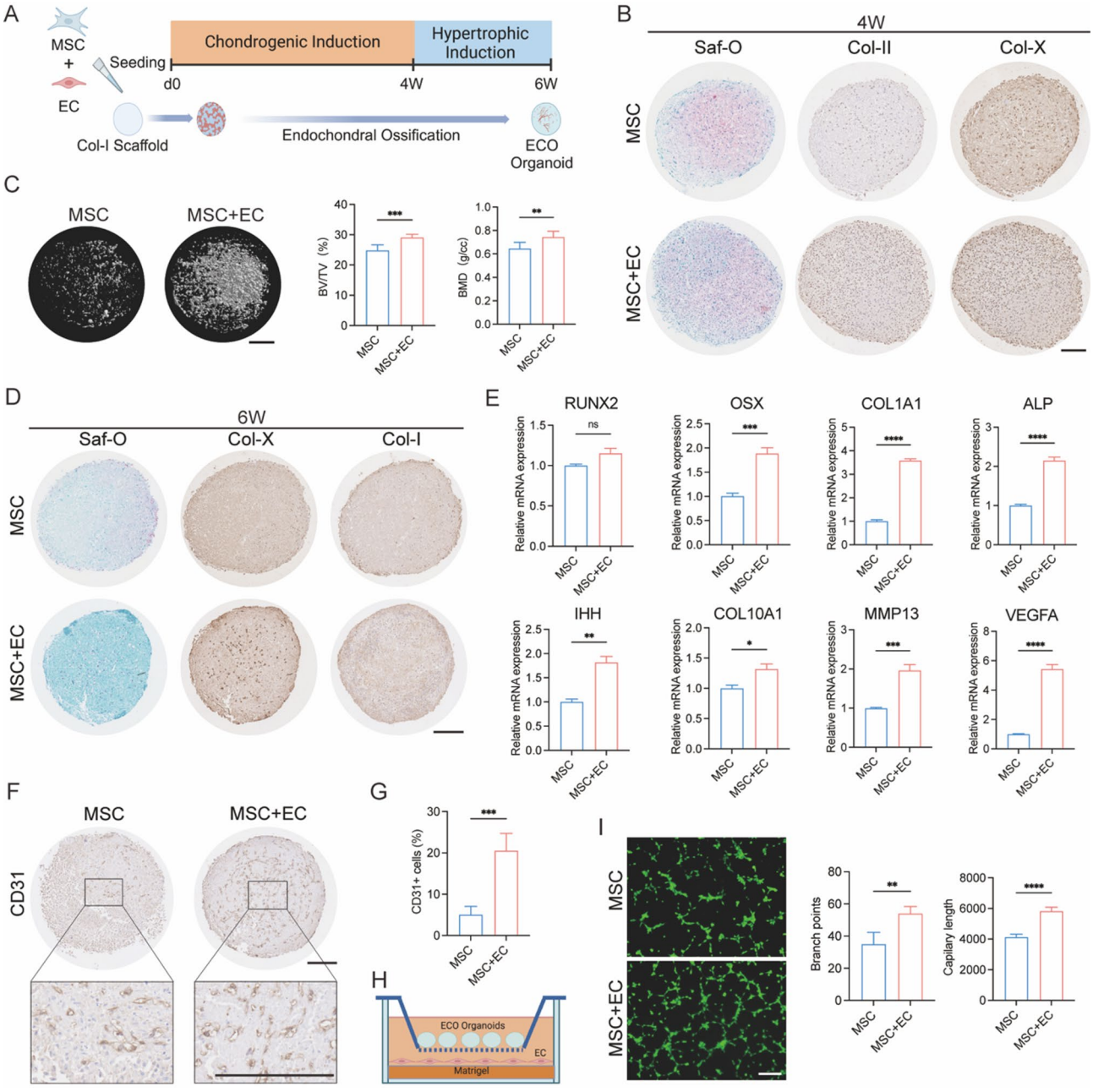


**Fig. 5** Results of endochondral osteogenesis in vitro. **A** ECO model overview diagram. **B** Results of section staining at 4 weeks: Safranin O-Fast Green staining and immunohistochemistry (Col-II and Col-X). **C** μ-CT results and quantification at 6 weeks suggests the mineralization level of the organoids. **D** Results of section staining at 6 weeks: Safranin O-Fast Green staining and immunohistochemistry (Col-X and Col-I). **E** RT-qPCR results at week 6 revealed the expression of bone and cartilage related genes. **F** CD31 immunohistochemical staining of ECO organoids at 6 weeks. **G** Quantitative results of the proportion of CD31-positive cells in ECO organoids at 6 weeks. **H** Schematic diagram of Transwell tube formation experiment. **I** The results of tube forming experiment revealed the effect of ECO organoid paracrine on angiogenesis of ECs. Scale bar = 200 μm for all microscopy images. For all charts, data are presented as means ± SEM (standard error of the mean), * $p < 0.05$, ** $p < 0.01$, *** $p < 0.01$, **** $p < 0.0001$, ns: no significance, $n \geq 3$ per group

group appeared to have been gradually replaced and had more Col-X positive areas (Fig. 5B), indicating a gradual transition to hypertrophic chondrogenic phenotype in both groups, similar to the results of chondrogenic pellet staining.

After 6 weeks, μ-CT analysis demonstrated that MSC + EC group exhibited enhanced mineralization (Fig. 5C). Histological and immunohistochemical staining of 6-week ECO sections revealed that the cartilage matrix in MSC + EC group was more extensively replaced compared to the MSC group. Although there was no

significant difference in the immunohistochemical staining for Col-I, the expression of Col-X was markedly increased in the co-culture group (Fig. 5D). RT-qPCR analysis further revealed that the expression levels of osteogenic markers and cartilage hypertrophy markers were significantly elevated in the co-culture group compared to the control group (Fig. 5E). At 6 weeks, the MSC + EC group had more CD31-positive cells than the control group (Fig. 5F-G). Hypertrophic chondrocytes secrete high levels of VEGFA, which promotes the formation of blood vessels and facilitates the transition to bone [5, 36]. To compare the paracrine effects on angiogenesis between the two groups, we performed a Transwell tube formation assay (Fig. 5H). The results indicated that the angiogenic potential of the MSC + EC group was significantly higher than that of the MSC group (Fig. 5I). These results suggest that ECs may contribute to vascularization and mineralization during ECO.

#### Effect of MSC-EC constructs in the repair of critical-sized calvarial bone defects

Having confirmed that the paracrine effects of ECs are conducive to MSC osteogenesis through mechanisms related to ECO, and that early introduction of ECs in an in vitro MSC organoid model of ECO effectively enhanced the progression of late-stage cartilage hypertrophy and osteogenic differentiation during extended culture, we proceeded to apply this approach for in vivo bone repair. MSC-EC injectable constructs were made by encapsulating MSCs and ECs at a ratio of 9:1 in commercially obtained gelatin microspheres as a delivery vehicle (Figure S4) [37]. The control groups were empty microspheres without cells (Ctrl) and microspheres seeded with MSCs only (MSC). The cell-seeded groups (MSC and MSC + EC) were pre-cultured in chondrogenic induction medium for 7 days before implantation in critical-sized rat calvarial bone defects (Fig. 6A). This type of in vivo defect was chosen for two reasons: (1) Calvarial bone is one of a few bones in the body that repairs by intramembranous ossification. The intentional choice of an intramembranous bone formation model would better illustrate the potential advantages of a therapeutic approach based on ECO, which would not normally occur at this anatomical site. (2) The use of long bone defect models in small animals is associated with numerous limitations, particularly since these often need to be created at load-bearing sites and hence require extensive stabilization (e.g., using metal plates) during healing. This introduces problems of stress shielding and lack of physiological loading in the defect area, often resulting in inconsistent and non-representative repair outcomes [38].

At 6 weeks post-implantation, Microfil perfusion results demonstrated a much higher density of neovascularization in the defect site for the MSC + EC group compared to both the Ctrl and MSC groups (Fig. 6B). At 12 weeks, μ-CT analysis indicated greatly enhanced mineralization in the MSC group compared to Ctrl, as shown through bone volume fraction (BV/TV) and bone mineral density (BMD), while values for the MSC + EC group significantly exceeded the other two groups (Fig. 6C). Improved mineralization in the MSC and MSC + EC groups was verified by double labeling with Calcein and ARS (Fig. 6F).

Histological and immunohistochemical staining were performed on the calvarial section samples at 12 weeks post-implantation (Fig. 6D-E). Based on the histological images, no obvious signs of inflammation were observed at the implantation site, which may be attributed to the immunomodulatory effects of MSCs. Immunohistochemical staining for PD-L1 was markedly stronger in both experimental groups compared to the control group, supporting our hypothesis (Figure S5). We can observe that, compared to the control group, both the MSC group and the MSC + EC group showed evidence of endochondral ossification, as reflected by the presence of more Col-II and Col-X positive areas as well as more positive regions in the Safranin O staining. Combined with histological staining results and Col-I immunohistochemistry, it was confirmed that the MSC + EC group exhibited significant repair effects. Furthermore, through CD31 and α-SMA immunostaining and quantitative analysis (Fig. 6F) of the repaired tissue, it was confirmed that the co-culture group significantly enhanced the vascularization in the repair area. The vWF immunohistochemical staining results further confirmed the enhanced level of vascularization in the MSC + EC treatment group (Figure S6).

In addition, we further examined the expression of human mitochondria using specific antibodies (Figure S7). No positive staining was observed in the control group, while scattered positive cells were detected in both the MSC and MSC + EC groups, indicating the presence of implanted human-derived cells within the newly formed tissue. Notably, in the MSC + EC group, positive cells were observed surrounding blood vessels, suggesting that the implanted ECs may have participated in the formation of new vessels.

We further assessed the rate of bone tissue mineralization at 12 weeks post-implantation (Fig. 6G). Compared to the control group, both the MSC and MSC + EC groups exhibited a significantly increased mineralization rate, which may be attributed to the implanted cells. However, no significant difference was detected between the two experimental groups.

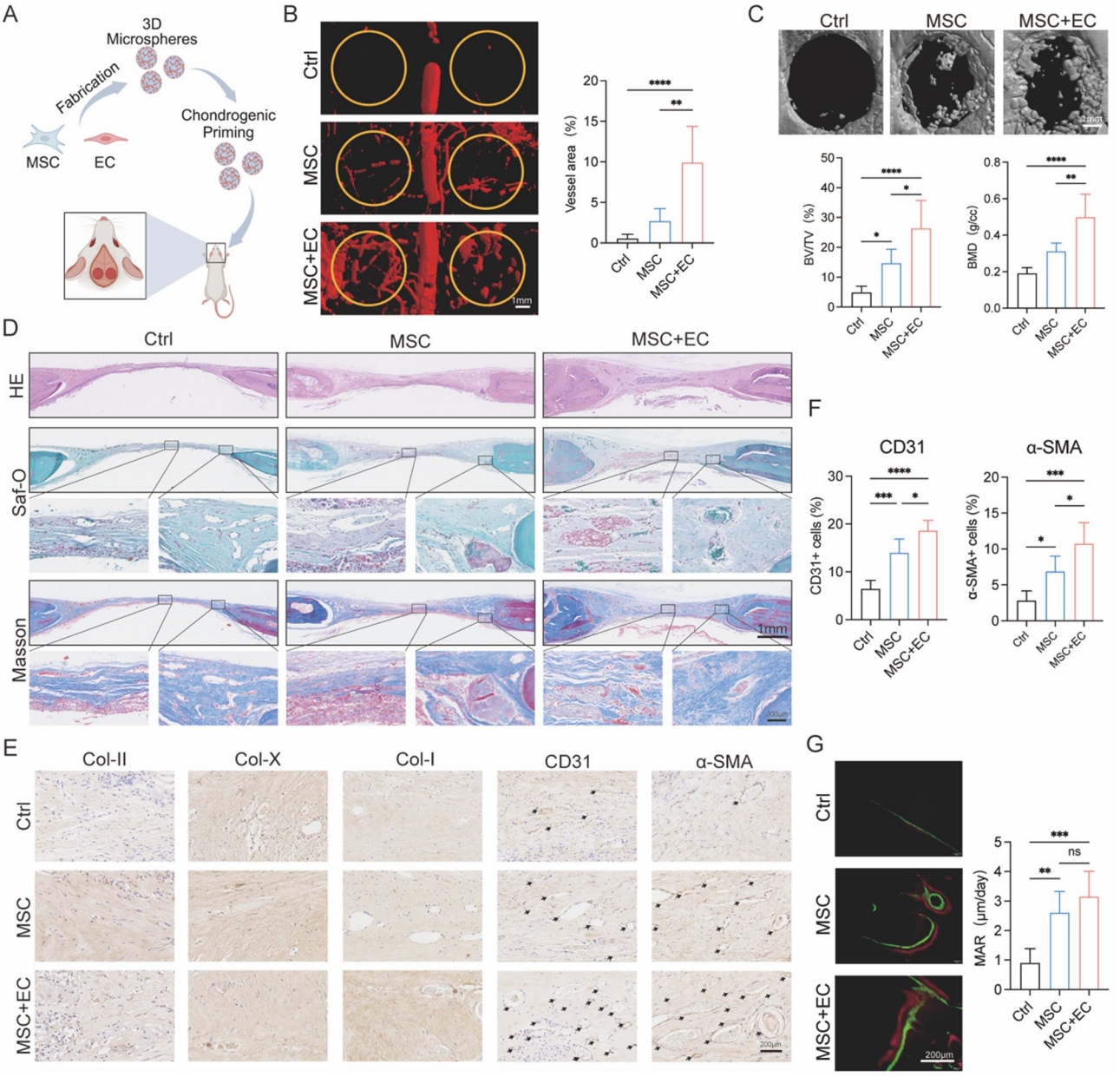


**Fig. 6** Evaluation of the effect of calvarial bone repair in vivo. **A** Schematic diagram of animal experiments. **B** Microfil perfusion imaging at 6 W revealed the level of vascularization in calvarial defect repair in different groups. **C** μ-CT scans revealed the effects of calvarial defect repair at 12 weeks. **D** Results of 12-week section histology staining: HE, Safranin O-Fast Green and Masson's trichrome. **E** Results of 12-week section immunohistology staining: Col-II, Col-X, Col-I, CD31 and α-SMA. **F** CD31 and α-SMA positive cell counts at 12 weeks revealed the level of vascularization in the repaired tissue. **G** Double labeling of Calcein and ARS at 12 weeks revealed the ability of bone mineralization. For all charts, data are presented as means ± SEM (standard error of the mean), * $p < 0.05$, ** $p < 0.01$, *** $p < 0.01$, **** $p < 0.0001$, ns: no significance, $n \geq 3$ per group

## Discussion

This study explored the role of MSC and EC co-culture in endochondral ossification (ECO), revealing a synergistic effect in angiogenesis, osteogenesis, and chondrocyte hypertrophy. When applied to tissue engineering strategies, this co-culture system enhanced in vitro osteogenesis and in vivo vascularized bone repair, suggesting it may serve as a promising bone tissue engineering (BTE) approach for critical-sized bone defects. Several key points are worth discussing.

Firstly, the importance of vascularization in ECO. ECO is a complex developmental process well documented over past decades [1, 2, 39–45]. Recent advances in bone tissue engineering have led to the establishment of ECO-based engineered models such as organoids or callus-like structures [25, 27, 46–52]. Unlike intramembranous ossification (IMO), ECO enables the formation

of more vascularized, biomimetic bone [53–55]. Considering the differential roles of vascularization in osteoarthritis (OA) and ECO [56–59], our study incorporated ECs into an established in vitro ECO organoid model [25]. Early inclusion of ECs in a 3D culture system successfully mimicked essential features of ECO, including late-stage hypertrophy, vascular ingrowth, and matrix mineralization.

Secondly, selection of MSC tissue source. It is noteworthy that this study selected human umbilical cord mesenchymal stem cells (UCMSCs) as the primary seed cells, due to their superior proliferative capacity and lower immunogenicity compared to MSCs derived from sources such as bone marrow or adipose tissue [60]. In addition, UCMSCs share the same tissue origin as ECs used in this study (HUVECs), which may help enhance cellular compatibility and functional interactions during co-culture. This "tissue-origin matching" strategy may be of particular significance for constructing vascularized tissues.

Thirdly, how MSCs enhance angiogenesis. In this study, we observed that MSCs promoted angiogenesis. This effect may be mediated through two primary mechanisms. First, MSCs can secrete a variety of pro-angiogenic factors, such as vascular endothelial growth factor A (VEGFA), fibroblast growth factor 2 (FGF2), platelet-derived growth factor subunit B (PDGFB), and hepatocyte growth factor (HGF), which enhance EC proliferation, migration, and tube formation, thereby promoting neovascularization [61, 62]. Second, there may be direct cell–cell contact between MSCs and ECs, which could further support spatial organization and stabilization of vascular structures through specific signaling pathways. Additionally, MSCs are widely recognized to exhibit pericyte (PC)-like characteristics. PCs are perivascular cells that naturally reside around capillaries and venules, and they regulate vessel formation, maturation, and stabilization through both direct contact and paracrine signaling with endothelial cells. During embryonic development and tissue repair, the coordination between ECs and PCs is essential for the formation of functional vasculature. This interaction primarily involves key signaling pathways such as VEGFA, Angiopoietin-1/Tie2, PDGFB, Notch, and TGF-β [63, 64]. These findings suggest that MSCs may promote angiogenesis through similar mechanisms.

Fourthly, how ECs promote chondrocyte hypertrophy. In this study, ECs were found to accelerate the hypertrophic progression of chondrocytes. According to transcriptomic analysis, this effect may be associated with the activation of the PI3K-AKT and TGF-β signaling pathways (Fig. 4). Interestingly, we found that co-culture with ECs upregulated Mmp13 and downregulated Ihh in ATDC5 cells. Since Ihh is typically expressed in early hypertrophy and declines at later stages, we speculate that ECs accelerated ATDC5 hypertrophy progression, explaining this expression pattern and suggesting ECs may facilitate cartilage-to-bone transition by promoting terminal maturation.

Fifthly, how MSC–EC interact within ECO organoids. Prior studies showed ECs promote MSC osteogenesis [13, 65]. ECs not only form bone vasculature and deliver nutrients, but also exert paracrine effects on osteoblasts, which in turn support EC angiogenesis [66–69]. In our 3D organoid system, ECs likely played paracrine roles in early ECO, co-differentiating with MSCs into hypertrophic chondrocytes. Later, some ECs may undergo apoptosis, while others form functional vessels, continuing to influence neighboring hypertrophic chondrocytes and osteoblasts/osteocytes.

Sixthly, the choice of in vivo model. We selected a calvarial defect model for its experimental simplicity and clear demonstration of ECO processes. Although calvarial bones primarily undergo IMO, chondrocyte presence during calvarial development [52] and ECO involvement in repair [57] have been reported. Thus, critical-sized calvarial defects can activate ECO, providing a suitable platform to study vascular–bone coupling and scaffold-mediated regeneration. Compared to long bone models, this approach also offers advantages in imaging, ethics, and animal welfare.

Lastly, limitations of this study. In vitro growth factor induction cannot fully mimic the complex in vivo microenvironment, potentially contributing to in vitro–in vivo discrepancies. In addition, although immunohistostaining confirmed human-derived cells in new vasculature in vivo (Figure S7), we did not trace the lineage of ECs in ECO Organoids in vitro. CD31 + cells observed in monocultures raise the question of whether ECs in ECO organoids derived from seeded ECs or differentiated from other sources. Future studies should address these dynamics for a deeper understanding of cell fate in ECO systems.

## Conclusion

In conclusion, the present study comprehensively elucidated the cellular interactions between MSCs and ECs during bone regeneration in ECO organoids and in vivo model. We firstly identified the influence of MSCs on the vascularization during ECO. Furthermore, ECs promoted the early hypertrophy of MSCs derived chondrocytes and their late transdifferentiation into osteocytes and matrix mineralization. Co-cultivation of MSCs and ECs synergistically enhanced the capacity of bone regeneration and in vivo bone repair efficacy by ECO. This study could provide valuable insights for strategies in bone tissue engineering in the future.

**Abbreviations**

| | |
|---|---|
| AKT | Protein kinase B (PKB) |
| ALP | Alkaline phosphatase |
| ARS | Alizarin Red S |
| CCK-8 | Cell counting kit-8 |
| Col-I | Collagen Type I |
| Col-II | Collagen Type II |
| Col-X | Collagen Type X |
| Ctrl | Control group |
| DAPI | 4′,6-Diamidino-2-phenylindole |
| EC | Endothelial cell |
| ECO | Endochondral ossification |
| FGF2 | Fibroblast growth factor 2 |
| HGF | Hepatocyte growth factor |
| IMO | Intramembranous ossification |
| MSC | Mesenchymal stem cell |
| PC | Pericyte |
| PDGFB | Platelet-derived growth factor subunit B |
| PD-L1 | Programmed death-ligand 1 (PD-L1) |
| PI3K | Phosphoinositide 3-kinase |
| Saf-O | Safranin O-Fast Green |
| SEM | Standard error of the mean |
| TGF-β3 | Transforming growth factor beta 3 |
| VEGFA | Vascular endothelial growth factor A |

## Supplementary Information

The online version contains supplementary material available at https://doi.org/10.1186/s13287-025-04733-4.

Additional file 1.

Additional file 2.

Additional file 3.

**Acknowledgments**

The authors deeply appreciate the efforts by their collaborators at the Arthritis Clinic & Research Center, Peking University People's Hospital, Peking University. The authors declare that they have not use AI-generated work in this manuscript.

**Author contributions**

YQS and ZHH contributed to the conception and design, collection and/or assembly of data, data analysis and interpretation, and manuscript writing. JJL contributed to data analysis and interpretation and final approval of the manuscript. QQC, DW, ZY, YY, LC and FHY contributed to the collection and/or assembly of data. JHL, HL, and DX provided financial support, administrative support, and final approval of the manuscript. All authors read and approved the final manuscript.

**Funding**

This research was funded by the National Key Research and Development Program of China (2022YFC2503103 and 2024YFA1108603), Natural Science Foundation of Beijing Municipality (L222087, L232094, and L244019), the National Natural Science Foundation of China (82302776) and Peking University People's Hospital Scientific Research Development Funds (RDGS2023-04, RDX2023-12, and RS2024-04).

**Data availability**

The RNA-seq data in this study has been uploaded to the NCBI SRA database (SRA accession number: PRJNA1227100). The other data and materials underlying this article will be shared on reasonable request to the corresponding author.

## Declarations

**Ethics approval and consent to participate**

The animal experiments were conducted under the approval of the Peking University Ethics Committee (LA2019365). (1) Title of the approved project: Analysis of key cells and significant characteristics of fibrous cartilage repair at different stages after microfracture surgery; (2) Name of the institutional approval committee or unit: Biomedical Ethics Committee of Peking University; (3) Approval number: LA2019365; (4) Date of approval: 2019-12-17. The study was reported following Animal Research: Reporting of In Vivo Experiments (ARRIVE) guidelines. The original source of the human cells used in this study (UCMSCs and HUVECs) has confirmed that the collection of these human cells was approved by an initial ethics review, and that the donors had signed informed consent.

**Consent for publication**

Written informed consent for publication was obtained from all participants.

**Competing interests**

The authors have declared that no competing interest exists.

Received: 18 February 2025 / Accepted: 3 October 2025
Published online: 18 November 2025

**References**

1. Saul D, Khosla S. Fracture healing in the setting of endocrine Diseases, Aging, and cellular senescence. Endocr Rev. 2022;43(6).
2. Long F, Ornitz DM. Development of the endochondral skeleton. Cold Spring Harb Perspect Biol. 2013;5(1):a008334.
3. Darbellay F, Ramisch A, Lopez-Delisle L, Kosicki M, Rauseo A, Jouini Z, Visel A, Andrey G. Pre-hypertrophic chondrogenic enhancer landscape of limb and axial skeleton development. Nat Commun. 2024;15(1):4820.
4. Tuckermann J, Adams RH. The endothelium-bone axis in development, homeostasis and bone and joint disease. Nat Rev Rheumatol. 2021;17(10):608–20.
5. Peng Y, Wu S, Li Y, Crane JL. Type H blood vessels in bone modeling and remodeling. Theranostics. 2020;10(1):426–36.
6. Dzamukova M, Brunner TM, Miotla-Zarebska J, Heinrich F, Brylka L, Mashreghi M-F, Kusumbe A, Kühn R, Schinke T, Vincent TL, Löhning M. Mechanical forces couple bone matrix mineralization with Inhibition of angiogenesis to limit adolescent bone growth. Nat Commun. 2022;13(1):3059.
7. Gonçalves RC, Banfi A, Oliveira MB, Mano JF. Strategies for re-vascularization and promotion of angiogenesis in trauma and disease. Biomaterials. 2021;269:120628.
8. Wang L, Fan H, Zhang Z-Y, Lou A-J, Pei G-X, Jiang S, Mu T-W, Qin J-J, Chen S-Y, Jin D. Osteogenesis and angiogenesis of tissue-engineered bone constructed by prevascularized β-tricalcium phosphate scaffold and mesenchymal stem cells. Biomaterials. 2010;31(36):9452–61.
9. Zou D, Zhang Z, He J, Zhang K, Ye D, Han W, Zhou J, Wang Y, Li Q, Liu X, Zhang X, Wang S, Hu J, Zhu C, Zhang W, zhou Y, Fu H, Huang Y, Jiang X. Blood vessel formation in the tissue-engineered bone with the constitutively active form of HIF-1α mediated BMSCs. Biomaterials. 2012;33(7):2097–108.
10. Street J, Bao M, deGuzman L, Bunting S, Peale FV, Ferrara N, Steinmetz H, Hoeffel J, Cleland JL, Daugherty A, van Bruggen N, Redmond HP, Carano RAD, Filvaroff EH. Vascular endothelial growth factor stimulates bone repair by promoting angiogenesis and bone turnover. Proc Natl Acad Sci U S A. 2002;99(15):9656–61.
11. Fan H, Zeng X, Wang X, Zhu R, Pei G. Efficacy of prevascularization for segmental bone defect repair using β-tricalcium phosphate scaffold in rhesus monkey. Biomaterials. 2014;35(26):7407–15.
12. Xu Z, Wang B, Huang R, Guo M, Han D, Yin L, Zhang X, Huang Y, Li X. Efforts to promote osteogenesis-angiogenesis coupling for bone tissue engineering. Biomater Sci. 2024;12(11):2801–30.
13. Heo DN, Hospodiuk M, Ozbolat IT. Synergistic interplay between human MSCs and HUVECs in 3D spheroids laden in collagen/fibrin hydrogels for bone tissue engineering. Acta Biomater. 2019;95:348–56.
14. Lu W, Li X, Wang Z, Zhao C, Li Q, Zhang L, Yang S. Mesenchymal stem cell-derived extracellular vesicles accelerate diabetic wound healing by inhibiting NET-induced ferroptosis of endothelial cells. Int J Biol Sci. 2024;20(9):3515–29.
15. Łabędź-Masłowska A, Vergori L, Kędracka-Krok S, Karnas E, Bobis-Wozowicz S, Sekuła-Stryjewska M, Sarna M, Andriantsitohaina R. Zuba-Surma, mesenchymal stem cell-derived extracellular vesicles exert pro-angiogenic and pro-lymphangiogenic effects in ischemic tissues by transferring various MicroRNAs and proteins including ITGa5 and NRP1. J Nanobiotechnol. 2024;22(1):60.

16. Xiao X, Xu M, Yu H, Wang L, Li X, Rak J, Wang S, Zhao RC. Mesenchymal stem cell-derived small extracellular vesicles mitigate oxidative stress-induced senescence in endothelial cells via regulation of miR-146a/Src. Signal Transduct Target Ther. 2021;6(1):354.
17. Wang Z, Han T, Zhu H, Tang J, Guo Y, Jin Y, Wang Y, Chen G, Gu N, Wang C. Potential osteoinductive effects of hydroxyapatite nanoparticles on mesenchymal stem cells by endothelial cell interaction. Nanoscale Res Lett. 2021;16(1):67.
18. Liu Y, Chen J, Liang H, Cai Y, Li X, Yan L, Zhou L, Shan L, Wang H. Human umbilical cord-derived mesenchymal stem cells not only ameliorate blood glucose but also protect vascular endothelium from diabetic damage through a paracrine mechanism mediated by MAPK/ERK signaling. Stem Cell Res Ther. 2022;13(1):258.
19. Freeman FE, Allen AB, Stevens HY, Guldberg RE, McNamara LM. Effects of in vitro endochondral priming and pre-vascularisation of human MSC cellular aggregates in vivo. Stem Cell Res Ther. 2015;6:218.
20. Lin Z, Zhang X, Fritch MR, Li Z, Kuang B, Alexander PG, Hao T, Cao G, Tan S, Bruce KK, Lin H. Engineering pre-vascularized bone-like tissue from human mesenchymal stem cells through simulating endochondral ossification. Biomaterials. 2022;283:121451.
21. Freeman FE, Brennan MÁ, Browe DC, Renaud A, De Lima J, Kelly DJ, McNamara LM, Layrolle P. A developmental Engineering-Based approach to bone repair: endochondral priming enhances vascularization and new bone formation in a critical size defect. Front Bioeng Biotechnol. 2020;8:230.
22. Freeman FE, Stevens HY, Owens P, Guldberg RE, McNamara LM. Osteogenic differentiation of mesenchymal stem cells by mimicking the cellular niche of the endochondral template. Tissue Eng Part A. 2016;22(19–20):1176–90.
23. Lv N, Zhou Z, Hou M, Hong L, Li H, Qian Z, Gao X, Liu M. Research progress of vascularization strategies of tissue-engineered bone. Front Bioeng Biotechnol. 2023;11:1291969.
24. Menger MM, Laschke MW, Orth M, Pohlemann T, Menger MD, Histing T. Vascularization strategies in the prevention of nonunion formation. Tissue Eng Part B Rev. 2021;27(2):107–32.
25. He Z, Li H, Zhang Y, Gao S, Liang K, Su Y, Du Y, Wang D, Xing D, Yang Z, Lin J. Enhanced bone regeneration via endochondral ossification using Exendin-4-modified mesenchymal stem cells. Bioact Mater. 2024;34.
26. Bao F, Yi J, Liu Y, Zhong Y, Zhang H, Wu Z, Heng BC, Wang Y, Wang Z, Xiao L, Liu H, Ouyang H, Zhou J. Free or fixed state of nHAP differentially regulates hBMSC morphology and osteogenesis through the valve role of ITGA7. Bioact Mater. 2022;18:539–51.
27. Zhang M, Shi J, Xie M, Wen J, Niibe K, Zhang X, Luo J, Yan R, Zhang Z, Egusa H, Jiang X. Recapitulation of cartilage/bone formation using iPSCs via biomimetic 3D rotary culture approach for developmental engineering. Biomaterials. 2020;260:120334.
28. Wen L, Yan W, Zhu L, Tang C, Wang G. The role of blood flow in vessel remodeling and its regulatory mechanism during developmental angiogenesis. Cell Mol Life Sci. 2023;80(6):162.
29. Shukunami C, Ishizeki K, Atsumi T, Ohta Y, Suzuki F, Hiraki Y. Cellular hypertrophy and calcification of embryonal carcinoma-derived chondrogenic cell line ATDC5 in vitro. J Bone Min Res. 1997;12(8):1174–88.
30. Newton PT, Staines KA, Spevak L, Boskey AL, Teixeira CC, Macrae VE, Canfield AE, Farquharson C. Chondrogenic ATDC5 cells: an optimised model for rapid and physiological matrix mineralisation. Int J Mol Med. 2012;30(5):1187–93.
31. Wang T, Zhang X, Bikle DD. Osteogenic differentiation of periosteal cells during fracture healing. J Cell Physiol. 2017;232(5):913–21.
32. Zhen G, Cao X. Targeting TGFβ signaling in subchondral bone and articular cartilage homeostasis. Trends Pharmacol Sci. 2014;35(5):227–36.
33. Wu M, Wu S, Chen W, Li Y-P. The roles and regulatory mechanisms of TGF-β and BMP signaling in bone and cartilage development, homeostasis and disease. Cell Res. 2024;34(2):101–23.
34. Raucci A, Bellosta P, Grassi R, Basilico C, Mansukhani A. Osteoblast proliferation or differentiation is regulated by relative strengths of opposing signaling pathways. J Cell Physiol. 2008;215(2):442–51.
35. Hellingman CA, Davidson ENB, Koevoet W, Vitters EL, van den Berg WB, van Osch GJVM, van der Kraan PM. Smad signaling determines chondrogenic differentiation of bone-marrow-derived mesenchymal stem cells: Inhibition of Smad1/5/8P prevents terminal differentiation and calcification. Tissue Eng Part A. 2011;17(7–8):1157–67.
36. Maes C. Signaling pathways effecting crosstalk between cartilage and adjacent tissues: seminars in cell and developmental biology: the biology and pathology of cartilage. Semin Cell Dev Biol. 2017;62:16–33.
37. Xing D, Liu W, Li JJ, Liu L, Guo A, Wang B, Yu H, Zhao Y, Chen Y, You Z, Lyu C, Li W, Liu A, Du Y, Lin J. Engineering 3D functional tissue constructs using self-assembling cell-laden microniches. Acta Biomater. 2020;114:170–82.
38. McGovern JA, Griffin M, Hutmacher DW. Animal models for bone tissue engineering and modelling disease. Dis Model Mech. 2018;11(4).
39. Yang L, Tsang KY, Tang HC, Chan D, Cheah KSE. Hypertrophic chondrocytes can become osteoblasts and osteocytes in endochondral bone formation. Proc Natl Acad Sci USA. 2014;111(33):12097–102.
40. Ayturk UM, Scollan JP, Goz Ayturk D, Suh ES, Vesprey A, Jacobsen CM, Divieti Pajevic P, Warman ML. Single-Cell RNA sequencing of calvarial and Long-Bone endocortical cells. J Bone Min Res. 2020;35(10):1981–91.
41. Wang H, Zheng C, Lu W, He T, Fan J, Wang C, Jie Q, Chan D, Cheah KSE, Yang L. Hedgehog signaling orchestrates cartilage-to-bone transition independently of smoothened. Matrix Biol. 2022;110:76–90.
42. Liu C-F, Lefebvre V. The transcription factors SOX9 and SOX5/SOX6 cooperate genome-wide through super-enhancers to drive chondrogenesis. Nucleic Acids Res. 2015;43(17):8183–203.
43. Tortelli F, Tasso R, Loiacono F, Cancedda R. The development of tissue-engineered bone of different origin through endochondral and intramembranous ossification following the implantation of mesenchymal stem cells and osteoblasts in a murine model. Biomaterials. 2010;31(2):242–9.
44. Zhong L, Huang X, Karperien M, Post JN. The regulatory role of signaling crosstalk in hypertrophy of MSCs and human articular chondrocytes. Int J Mol Sci. 2015;16(8):19225–47.
45. Zhang X, Jiang W, Xie C, Wu X, Ren Q, Wang F, Shen X, Hong Y, Wu H, Liao Y, Zhang Y, Liang R, Sun W, Gu Y, Zhang T, Chen Y, Wei W, Zhang S, Zou W, Ouyang H. Msx1 + stem cells recruited by bioactive tissue engineering graft for bone regeneration. Nat Commun. 2022;13(1):5211.
46. Scotti C, Tonnarelli B, Papadimitropoulos A, Scherberich A, Schaeren S, Schauerte A, Lopez-Rios J, Zeller R, Barbero A, Martin I. Recapitulation of endochondral bone formation using human adult mesenchymal stem cells as a paradigm for developmental engineering. Proc Natl Acad Sci USA. 2010;107(16):7251–6.
47. Scotti C, Piccinini E, Takizawa H, Todorov A, Bourgine P, Papadimitropoulos A, Barbero A, Manz MG, Martin I. Engineering of a functional bone organ through endochondral ossification. Proc Natl Acad Sci USA. 2013;110(10):3997–4002.
48. Nilsson Hall G, Mendes LF, Gklava C, Geris L, Luyten FP, Papantoniou I. Developmentally engineered callus organoid bioassemblies exhibit predictive in vivo long bone healing. Adv Sci (Weinheim Baden-Wurttemberg Germany). 2020;7(2):1902295.
49. Pigeot S, Klein T, Gullotta F, Dupard SJ, Garcia Garcia A, García-García A, Prithiviraj S, Lorenzo P, Filippi M, Jaquiery C, Kouba L, Asnaghi MA, Raina DB, Dasen B, Isaksson H, Önnerfjord P, Tägil M, Bondanza A, Martin I, Bourgine PE. Manufacturing of human tissues as off-the-Shelf grafts programmed to induce regeneration. Adv Mater. 2021;33(43):e2103737.
50. Xie C, Liang R, Ye J, Peng Z, Sun H, Zhu Q, Shen X, Hong Y, Wu H, Sun W, Yao X, Li J, Zhang S, Zhang X, Ouyang H. High-efficient engineering of osteo-callus organoids for rapid bone regeneration within one month. Biomaterials. 2022;288:121741.
51. Morimoto S, Kajiya M, Yoshii H, Yoshino M, Horikoshi S, Motoike S, Iwata T, Ouhara K, Ando T, Yoshimoto T, Shintani T, Mizuno N. A cartilaginous construct with bone collar exerts bone-Regenerative property via rapid endochondral ossification. Stem Cell Reviews Rep. 2023;19(6):1812–27.
52. Wei X, Qiu J, Lai R, Wei T, Lin Z, Huang S, Jiang Y, Kuang Z, Zeng H, Gong Y, Xie X, Yang J, Zhang Y, Zhang S, Zou Z, Gao X, Bai X. A human organoid drug screen identifies α2-adrenergic receptor signaling as a therapeutic target for cartilage regeneration. Cell Stem Cell. 2024.
53. Sun L, Niu H, Wu Y, Dong S, Li X, Kim BYS, Liu C, Ma Y, Jiang W, Yuan Y. Bio-integrated scaffold facilitates large bone regeneration dominated by endochondral ossification. Bioact Mater. 2024;35:208–27.
54. Liu Y, Kuang B, Rothrauff BB, Tuan RS, Lin H. Robust bone regeneration through endochondral ossification of human mesenchymal stem cells within their own extracellular matrix. Biomaterials. 2019;218:119336.
55. Gao J, Wang H, Li M, Liu Z, Cheng J, Liu X, Liu J, Wang X, Zhang L. DLP-printed GelMA-PMAA scaffold for bone regeneration through endochondral ossification. Int J Bioprinting. 2023;9(5):754.
56. Charlier E, Deroyer C, Ciregia F, Malaise O, Neuville S, Plener Z, Malaise M, de Seny D. Chondrocyte dedifferentiation and osteoarthritis (OA). Biochem Pharmacol. 2019;165:49–65.
57. Rim YA, Nam Y, Ju JH. The role of chondrocyte hypertrophy and senescence in osteoarthritis initiation and progression. Int J Mol Sci. 2020;21(7).

58. Horváth E, Sólyom Á, Székely J, Nagy EE, Popoviciu H. Inflammatory and metabolic signaling interfaces of the hypertrophic and senescent chondrocyte phenotypes associated with osteoarthritis. Int J Mol Sci. 2023;24(22).
59. Fan Y, Bian X, Meng X, Li L, Fu L, Zhang Y, Wang L, Zhang Y, Gao D, Guo X, Lammi MJ, Peng G, Sun S. Unveiling inflammatory and prehypertrophic cell populations as key contributors to knee cartilage degeneration in osteoarthritis using multi-omics data integration. Ann Rheum Dis. 2024;83(7):926–44.
60. Zhang S, Wang JY, Li B, Yin F, Liu H. Single-cell transcriptome analysis of uncultured human umbilical cord mesenchymal stem cells. Stem Cell Res Ther. 2021;12(1):25.
61. Lin H, Chen H, Zhao X, Chen Z, Zhang P, Tian Y, Wang Y, Ding T, Wang L, Shen Y. Advances in mesenchymal stem cell conditioned medium-mediated periodontal tissue regeneration. J Translational Med. 2021;19(1):456.
62. Matsuzaka Y, Yashiro R. Therapeutic strategy of Mesenchymal-Stem-Cell-Derived extracellular vesicles as regenerative medicine. Int J Mol Sci. 2022;23(12):6480.
63. Bertani G, Di Tinco R, Bertoni L, Orlandi G, Pisciotta A, Rosa R, Rigamonti L, Signore M, Bertacchini J, Sena P, De Biasi S, Villa E, Carnevale G. Flow-dependent shear stress affects the biological properties of pericyte-like cells isolated from human dental pulp. Stem Cell Res Ther. 2023;14(1):31.
64. Li G, Gao J, Ding P, Gao Y. The role of endothelial cell-pericyte interactions in vascularization and diseases. J Adv Res. 2025;67:269–88.
65. Villars F, Guillotin B, Amédée T, Dutoya S, Bordenave L, Bareille R, Amédée J. Effect of HUVEC on human osteoprogenitor cell differentiation needs heterotypic gap junction communication. Am J Physiol Cell Physiol. 2002;282(4):C775–85.
66. Goring A, Sharma A, Javaheri B, Smith RC, Kanczler JM, Boyde A, Hesse E, Mahajan S, Olsen BR, Pitsillides AA, Schneider P, Oreffo RO, Clarkin CE. Regulation of the bone vascular network is sexually dimorphic. J Bone Min Res. 2019;34(11):2117–32.
67. Neag G, Finlay M, Naylor AJ. The cellular choreography of osteoblast angiotropism in bone development and homeostasis. Int J Mol Sci. 2021;22(14).
68. Liao P, Chen L, Zhou H, Mei J, Chen Z, Wang B, Feng JQ, Li G, Tong S, Zhou J, Zhu S, Qian Y, Zong Y, Zou W, Li H, Zhang W, Yao M, Ma Y, Ding P, Pang Y, Gao C, Mei J, Zhang S, Zhang C, Liu D, Zheng M, Gao J. Osteocyte mitochondria regulate angiogenesis of transcortical vessels. Nat Commun. 2024;15(1):2529.
69. Song H, Li X, Zhao Z, Qian J, Wang Y, Cui J, Weng W, Cao L, Chen X, Hu Y, Su J. Reversal of osteoporotic activity by endothelial Cell-Secreted bone targeting and biocompatible exosomes. Nano Lett. 2019;19(5):3040–8.

## Publisher's note